COMMUNICATION

Seedless synthesis of patterned ZnO nanowire arrays on metal thin films (Au, Ag, Cu, Sn) and their application for flexible electromechanical sensing

Xiaonan Wen, Wenzhuo Wu, Yong Ding and Zhong Lin Wang*

The synthesis of high quality ZnO nanowire (NW) arrays on a range of conventional conductive substrates has important applications in LEDs, nanogenerators and piezotronics. In this paper, using ammonium hydroxide as the reactant, together with zinc nitrate hexahydrate, ZnO NW arrays have been grown on various patterned metal layers, such as Au, Ag, Cu and Sn, without pre-depositing a seed layer. The mechanism for this novel synthesis route has been discussed and the effect of parameters such as ammonia concentration and solution/container volume ratio on the nanowire growth has also been investigated. Preferentially selective nucleation and the subsequent growth of ZnO NW arrays was demonstrated on patterns of different metals without a ZnO seed. Electrical characterization was subsequently performed to reveal the characteristics of the contacts formed between the ZnO NWs and the underlying metal layer. Further demonstration of the as-fabricated ZnO NW arrays on flexible substrates as an electromechanical switch in response to externally applied strain exhibits the potential applications of the demonstrated seedless synthesis of patterned ZnO NW arrays in areas ranging from sensing, and energy harvesting to interfacing piezotronics with silicon based technologies.

1. Introduction

Wurtzite structured ZnO is an important semiconductor material with a wide direct bandgap (3.7 eV) and piezoelectric properties, and exhibits potential for novel applications by coupling the interdisciplinary fields of electronics, photonics and piezoelectricity.[1,2] The synthesis of aligned ZnO nanowire (NW) arrays has been studied[3,4] during the past several years due to the various potential applications of aligned ZnO NW arrays in light emitting diodes,[5–7] lasers,[8,9] solar cells,[10–12] nanogenerators[13–15] and piezotronics,[16,17] *etc.* Various methods have been reported for synthesizing ZnO NW arrays, mainly including physical vapor phase transport and deposition,[18–20] metal organic chemical vapor deposition (MOCVD)[21,22] and a hydrothermal approach.[23–25] In contrast to the physical deposition and MOCVD methods, which require high operation temperatures and are limited to certain inorganic substrates, the hydrothermal

School of Material Science and Engineering, Georgia Institute of Technology, Atlanta, Georgia 30332-0245, United States. E-mail: zlwang@gatech.edu

approach has been attracting increasing attention due to its flexibility for synthesizing ZnO NW arrays on a wide range of substrates at low cost and the potential of scaling up. For most of the hydrothermal approaches reported, a seed layer, normally a pre-deposited ZnO thin film, is indispensable to facilitate the nucleation and subsequent growth.[26] However, under certain circumstances, a seed layer may not be desirable due to the initial growth of a thin layer of ZnO film, in between the as-grown NWs and the substrate, which makes the roots of the NWs fuse together and hence renders indirect contact between the NWs and the substrate.
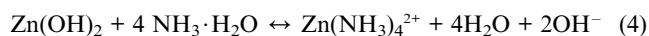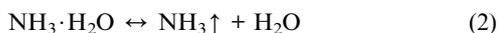
In this work, we report a novel hydrothermal approach for synthesizing aligned ZnO NW arrays preferentially on patterned surfaces of various commonly used metals without using a ZnO seed layer. Effects of experimental parameters such as the precursor concentration and the solution/container volume ratio in the chemical synthesis container have been studied. Electrical characterization was subsequently performed to reveal the characteristics of the contacts formed between the ZnO NWs and the metal layers. Further demonstration of the as-fabricated ZnO NW arrays on underlying flexible polyethylene terephthalate (PET) substrates as electromechanical switches/sensors in response to externally applied strain exhibits the potential applications of the demonstrated seedless synthesis of patterned ZnO NW arrays, in areas ranging from sensing,[27,28] and electromechanical actuation[29–31] to energy harvesting.[15,32–34]

2. Results and discussion

In contrast to the commonly reported hydrothermal synthesis that utilizes a combination of zinc nitrate hexahydrate and hexamethylenetetramine (HMTA) and makes use of the slow hydrolyzation of HMTA to provide a weak base environment,[4,35,36] here we use ammonium hydroxide instead, providing a relatively strong base environment. When ammonium hydroxide was firstly introduced into the solution, $Zn(OH)_2$ sediment was formed. By agitating the solution for a few seconds, it became clear again, indicating that the Zn^{2+} ions had combined with NH_4^+ ions to form stable zinc ammine.[37] HMTA hence provides a buffering mechanism for slowly releasing OH^-, while ammonium hydroxide enables a buffering mechanism of slowly releasing Zn^{2+}. Both methods can result in ZnO NW growth, while the method we present here results in unique properties as discussed later.

Some typical chemical reactions involved are listed below to describe the growth process:[38]

$$NH_3 \cdot H_2O \leftrightarrow NH_4^+ + OH^- \quad (1)$$

$$NH_3 \cdot H_2O \leftrightarrow NH_3\uparrow + H_2O \quad (2)$$

$$Zn^{2+} + 2OH^- \leftrightarrow Zn(OH)_2\downarrow \quad (3)$$

$$Zn(OH)_2 + 4 NH_3 \cdot H_2O \leftrightarrow Zn(NH_3)_4^{2+} + 4H_2O + 2OH^- \quad (4)$$

$$Zn(OH)_2 \leftrightarrow ZnO + H_2O \quad (5)$$

All of these chemical reactions are collectively in dynamic equilibrium and varying any one of them would affect the synthesis outcome. Factors affecting the reaction equilibrium include growth temperature, growth time, precursor concentration, the amount of ammonia gas dissolved in air in the container, *etc.* In this work, the effects of manipulating reaction (4) and reaction (2) by tuning the concentration of ammonium hydroxide and the solution/container (s/c) volume ratio are investigated in detail.

A. Concentration of ammonium hydroxide

Ammonium hydroxide plays a two-fold role in the growth process. First, it provides OH^-, which is the source of O in ZnO; second, it provides NH_4^+, which can form a complex with zinc ions as a buffering mechanism. In this section, the volume of the solution with 20 mM $Zn(NO_3)_2 \cdot 6H_2O$ was fixed at 350 ml, contained in a 500 ml reaction container while different amounts of ammonium hydroxide (28 wt%) was added into the solution, ranging from 2 ml to 20 ml, with the ammonium hydroxide/$Zn(NO_3)_2 \cdot 6H_2O$ nutrient solution volume ratio (named as the a/n volume ratio in this work) ranged from 0.57% to 5.71%. In general, the length of the as-grown NWs is determined by the total amount of source material available (namely Zn^{2+} and OH^-), the growth time and the release rate of Zn^{2+}. The diameter of the NWs is determined by the total amount of source material and the release rate of Zn^{2+}. In particular, the equilibrium status of reaction (4) has a significant effect in shaping the NW tips. The density of the as-grown NWs is determined by various factors, such as the number of nucleation sites generated on the substrate during the initial stage of growth, the extent of NW fusing and the diameter of the base of NWs, and is thus related to the amount of OH^- available, Zn^{2+} released initially, the total amount of source material available, and the growth time.

Fig. 1(a) shows SEM images of NWs grown at a 0.57% a/n volume ratio. NH_4^+ and OH^- were both insufficient in this case, especially since there was not enough NH_4^+ to consume all of the $Zn(OH)_2$, leaving the solution in a turbid condition. Thus there was no buffering at the initial stage of growth and the existing $Zn(OH)_2$ would rapidly decompose into ZnO once heated, resulting in a film-like structure deposited on the substrate, with some of the nanorods fused together, while the rest were still separated, as can be seen from Fig. 1(a). The diameters and lengths of the as-grown nanorods were small in this case due to an insufficient supply of source materials. When the a/n volume ratio was increased, the Zn^{2+} was more and more slowly released while the concentration of OH^- was increased in the solution. Since Zn^{2+} and OH^- are both the source materials for synthesizing ZnO NWs and the increase in OH^- concentration is accompanied by the decrease of free Zn^{2+} concentration, we thus

expect that with the increase of a/n ratio, the tip diameter, length and density of the NWs will increase to a maximum value first and decrease later. Fig. 1(b) and (c) show the results for NWs grown at 2.86% and 3.43% a/n volume ratios, respectively, which exhibit a good alignment and increase in tip diameter, length and density of NWs. By further increasing the a/n ratio, more source material would be available in the solution. However, not all of the three morphological parameters of the NW array increase. The length of the as-grown NWs increased due to faster vertical growth. The density of the NW array, however, decreased since small nuclei were likely to fuse with each other due to the faster deposition of ZnO occurring in the initial nucleation stage. As for the tip diameters of the NWs, the equilibrium of reaction (4) will shift to the right-hand side and the equilibrium of reaction (5) will shift to the left-hand side at a high a/n volume ratio. This means that there will be a higher etching rate of the formed ZnO crystal by ammonia. However, the etching is anisotropic because the absorption of NH_3 molecules is curvature dependent.[39] Regions of high curvature, such as the NW tips, attract more NH_3 molecules than the NW side walls and consequently such regions will be etched faster, resulting in needle-like NWs, as shown in Fig. 1(d). This phenomenon is named as the shaping effect in this work for convenience. Once the ammonium hydroxide concentration was increased to 5.71%, there was enough NH_4^+ in the solution that formed a complex with almost all of the Zn^{2+} ions and significantly depressed the growth process. As a result, no obvious growth of NWs can be observed, as shown in Fig. 1(e). Finally, a control experiment was performed for comparison, by using 350 ml solution of 20 mM $Zn(NO_3)_2 \cdot 6H_2O$ and 20 mM HMTA mixture, with the results shown in Fig. 1(f). A significant difference can be observed in that the NWs grown with the control recipe have larger dimensions, while the alignment among the NWs is poor. This could be explained by the difference in solution environment. In the control recipe, Zn^{2+} is in abundant existence while in the $Zn(NO_3)_2 \cdot 6H_2O + NH_3 \cdot H_2O$ recipe, there is only a limited amount of free Zn^{2+}, which greatly suppresses homogeneous nucleation and facilitates heterogeneous nucleation, leading to more nucleation sites on seedless substrates.[40]

Lastly, a group of experiments were carried out with different a/n volume ratios of 0.57%, 1.71%, 2.29%, 2.86%, 3.43%, 4.00%, 4.57%, 5.14%, and 5.71%. By examining three areas ($\sim$16 μm^2) around the center of a substrate with the as-grown NWs, the average diameter, length and density were obtained and plotted in Fig. 1(g), (h) and (i) to show the dependence relationship of these parameters on the ammonium hydroxide concentration. The NW array density reaches its maximum at $\sim$3.43% and the NW length reaches its maximum at $\sim$5.14%. The diameters of the NW tips reach a maximum of $\sim$147 nm at $\sim$2.86% and can be decreased to $\sim$20 nm at $\sim$5.14%. Our results provide a helpful guide of how to use the parameters of the a/n volume ratio or the ammonium hydroxide concentration, to engineer the synthesis process for the desired or optimized morphology of the grown ZnO NW arrays.

B. Solution/container volume ratio

Ammonia hydroxide (28 wt%) is an extremely volatile chemical especially under high temperature. There are three states of ammonia in our reaction system: ammonia ions, ammonia dissolved in the solution and ammonia vapor in the air. A number of factors can affect the equilibrium among these three states. In this section, the concentration of $Zn(NO_3)_2 \cdot 6H_2O$ was kept at 20 mM and the
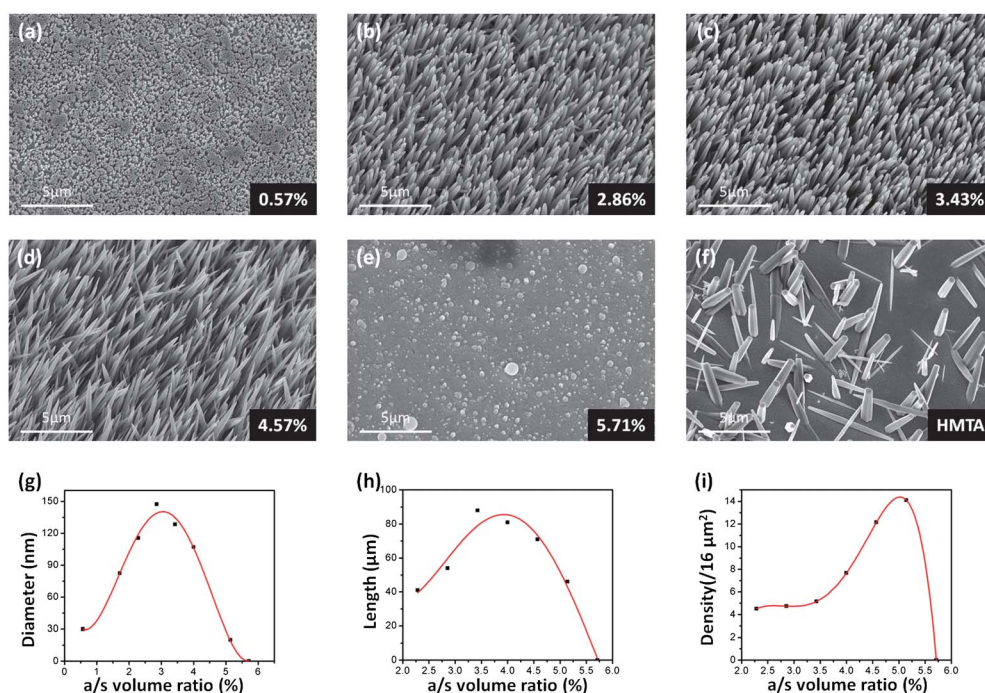
Fig. 1 Effects of ammonium hydroxide concentration (a/n volume ratio) on the morphology of ZnO NWs grown on seedless gold layer. (a)-(e) SEM images of NWs grown under a/n volume ratios of 0.57%, 2.86%, 3.43%, 4.57%, and 5.71%, respectively. The scale bar is 5 μm. (f) SEM image of NWs grown with the control recipe of $Zn(NO_3)_2 \cdot 6H_2O$ + HMTA. (g)-(i) Dependence relationship of NW tip diameters, length and density on the a/n volume ratio.

concentration of ammonia hydroxide was kept at 2.5% of the a/n volume ratio. The factor that changes is the volume of the solution, which tunes the equilibrium status of ammonia among the three states. Fig. 2(a) shows the result when the solution volume was kept at a low level of 25 ml in a 500 ml container. A relatively large amount of ammonia would therefore exist as vapor in the free space of the container before an equilibrium partial pressure can be reached, which might lead to a lower level of ammonia concentration (a/n volume ratio) in the solution. However, this does not result in a faster release of Zn^{2+}, since ammonia dissolved in the air will dissolve back into the solution through dynamic equilibrium. This is another buffering mechanism different from the one discussed in section A. Here, the new buffering mechanism helps keep the concentration of both Zn^{2+} and OH^- at a relatively low level, further slowing down the reaction rate, resulting in short but better-aligned NWs, as observed. The diameters of the NW tips were large and the shaping effect can be considered negligible, with the absence of a high level of NH_4^+ concentration. Fig. 2(b) shows the result when the solution volume was increased to 100 ml. The growth of NWs was faster and good alignment was maintained under this condition. The density of NWs decreased, however, due to a shorter nucleation stage and the average length of the NWs was dramatically increased from ~2 μm to ~9 μm due to faster growth, while the diameters of the NW tips were slightly decreased due to a weak shaping effect. Fig. 2(c) shows the result when the solution volume was further increased to 300 ml. Following the same trend as discussed above, the density of NWs further decreased while the length of the NWs slightly increased. Needle-like tips occurred for the as-grown NWs due to the significant shaping effect caused by abundant NH_4^+ in the solution.

Then the as-grown ZnO NWs under several different synthesis conditions were characterized using TEM. The HRTEM images and diffraction pattern obtained show that the ZnO NWs are single crystalline and possess the [0001] orientation along their growth directions regardless of the different synthesis conditions. One set of these images is given in Fig. 2(d), (e) and (f).

Lastly, a group of experiments were carried out with different s/c volume ratios of 0.05, 0.1, 0.2, 0.3, 0.4, 0.5, 0.6 and 0.7. By examining three areas (~16 μm²) around the center of a substrate with the as-grown NWs, the average diameter, length and density of the as-grown NWs are obtained and plotted in Fig. 2(g), (h) and (i) to show the dependence relationship of these parameters on the s/c volume ratio. The tip diameters and density of NWs increase monotonically with the decrease of the s/c volume ratio. The NW length, although it decreases with the decrease of s/c volume ratio, stays generally stable within the range of 0.2–0.6 s/c volume ratio.

In the above discussion, in addition to the conventionally investigated parameters like temperature, precursor concentration, growth time *etc.*, a new parameter, the partial pressure of ammonia in air has been investigated in detail. The results presented here suggest that by simply manipulating the partial pressure of ammonia gas together with others, the synthesis of ZnO NW arrays of desired morphology can be engineered and optimized in a controlled manner.

C. Patterned growth of ZnO NW arrays on different metal surfaces

Stronger nucleation is one of the advantages of the seedless hydro-thermal synthesis method reported here as compared to the control recipe in section A, which was reported previously in other work.[41] To demonstrate the capability of this seedless selective NW growth, ZnO NW arrays were synthesized seedlessly on substrates with pre-patterned metal electrodes. It was found that ZnO would not nucleate
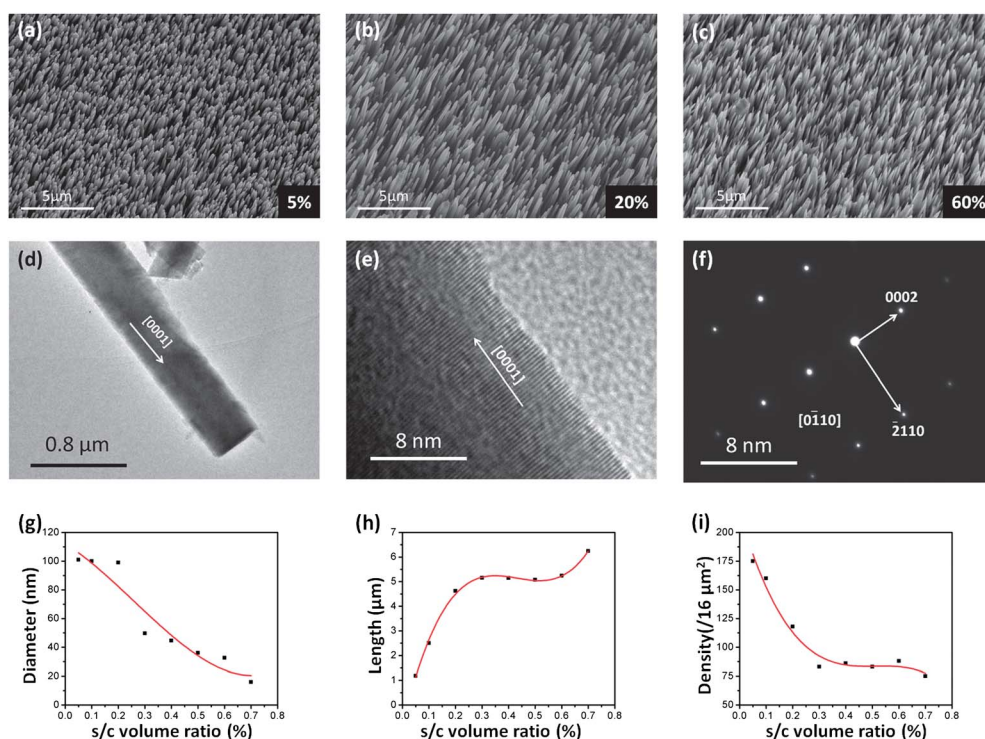
Fig. 2 Effects of solution/container volume ratio on the morphology of ZnO NWs grown on a seedless gold layer. (a)–(c) SEM images of NWs grown under different solution/container volume ratios 5%, 20% and 60%. The scale bar is 5 μm. (d) TEM image of a single ZnO NW. The arrow shows its [0001] crystal orientation. The scale bar is 0.8 μm. (e) HRTEM image of a single ZnO NW, indicating its single crystallinity. The arrow shows its [0001] crystal orientation. The scale bar is 8 nm. (f) Diffraction pattern of a single ZnO NW. The crystal orientation is shown in the image. The scale bar is 8 nm. (g)–(i) Dependence relationship of NW tip diameters, lengths and density on solution/container volume ratio.

on silicon dioxide while significant growth of NWs on areas deposited with suitable metals was observed. Fig. 3(a), (b), (c) and (d) show the SEM images of the as-grown NWs on patterned electrodes of gold, copper, silver and tin, respectively. The insets are the magnified images of the NW array for each case. No post-annealing process was performed for the copper, silver and tin electrodes. The results show that the aligned ZnO NW array can grow selectively and

preferentially on these metals, which enables the potential application of this synthesis method for fabricating ZnO NW arrays site-selectively on integrated circuits, which possess a vast amount of, for instance, copper electrodes and interconnects, in a well-controlled manner. This may pave the way for realizing the novel integration of semiconductor NW based piezotronics with state-of-the-art microelectronic technology and strategically coupling the optical, electrical and piezoelectric properties of semiconductor nanomaterials with the high speed computing/processing capability of integrated circuits.
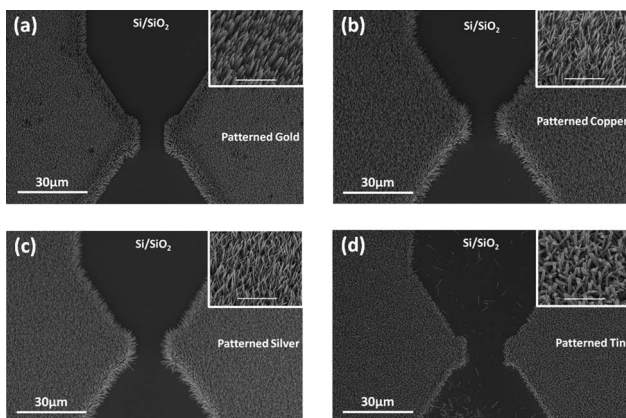
D. Contact characteristics between ZnO NWs and the underlying metals

ZnO NWs can form contacts with metal electrodes in different ways. The NWs can be placed on a flat substrate with metal electrodes deposited covering the two ends of the NW. Alternatively, the NWs can grow on the seed layer, which is in contact with the metal electrodes. A third possibility is that NWs can grow directly on a metal layer without pre-depositing a ZnO seed, as presented here in our work. The first method is usually adopted for ensuring the contact quality, mostly for single wire devices. It is, however, extremely difficult to assemble the NWs in an ordered manner, which hinders their utilization in large scale applications. In the second method, the pre-deposited seed layer can complicate the contact properties between the NWs and the metal layer, while the method presented here can potentially enable the large scale fabrication of NW arrays by avoiding both the intricate assembly step and the indirect contact formed between the NWs and metals due to the seeding layer.

Fig. 3 SEM images of the as-grown NWs on patterned metal electrodes. The scale bars for the four figures are 30 μm. The scale bars for the four insets are 6 μm. (a) NWs grown on gold electrodes. (b) NWs grown on copper electrodes. (c) NWs grown on silver electrodes. (d) NWs grown on tin electrodes. Insets are the magnified images of the NWs for each case.

The inset of Fig. 4(a) shows a schematic diagram of the as-fabricated device used for the electrical measurements. Chromium is used as an adhesion metal and also a capping metal for controllably prohibiting the growth of ZnO NWs, since ZnO NWs cannot grow hydrothermally on a chromium surface.[42] A third metal layer was deposited in between, and the exposed sides provided sites for ZnO to nucleate and grow. The gap between the two electrodes is 5 μm. Lastly, NWs from the two sides will meet and contact with each other after a sufficiently long growth time, as is shown in Fig. 4(a). Two types of contact exist in this structure. One is the metal–ZnO NW contact at the two ends and the other is the ZnO NW–ZnO NW contact in the middle. Considering that the NWs were grown under exactly the same conditions and especially that their physical distance during the growth process was only 5 μm at its maximum, it is reasonable to assume that there is a negligible difference in the dopant concentrations as well as the Fermi levels and hence the contact barrier should also be negligible between the ZnO NWs. As a result, the I–V curves obtained essentially reveal the characteristics of the metal–ZnO NW contact.

The I–V curve obtained from the Au-ZnO NW-ZnO NW-Au structure is shown in Fig. 4(b). The electron affinity of ZnO is 4.5 eV[32] and the work function of Au ranges from 5.1 eV to 5.47 eV.[43] Theoretically, they should form a Schottky contact[44] and the I–V curve obtained does show the rectifying character of Schottky contacts at both ends, with different barrier heights. The I–V curve for the Cu-ZnO NW-ZnO NW-Cu structure is shown in Fig. 4(c).

The work function of Cu ranges from 4.53 eV to 5.10 eV[40] and the I–V curve shows character of a weaker rectification behavior, which is consistent with the lower work function of copper. Fig. 4(d) is obtained from the Ag-ZnO NW-ZnO NW-Ag structure. The work function of Ag ranges from 4.52 eV to 4.74 eV,[40] which is very close to the electron affinity of ZnO. In consistency, the I–V curve shows the weakest rectification characters among the three.

The results of the electrical measurements show that the contact between the grown NWs and the underlying metal layer is accordant with theoretical predictions. It then suggests that our method provides a reliable alternative of making electrical contacts between metal electrodes and ZnO NWs, without the necessity for NW assembly and with the benefit of easy scale-up.

E. Electromechanical switch/sensor

Most of the seedless growths of ZnO NWs reported previously were performed on rigid substrates. With the method reported here, we can extend the seedless synthesis of large scale ZnO NW arrays from rigid substrates like silicon further to flexible ones such as PET, of which the applications of flexible electronic devices have drawn increasing attention recently.[45] Here, an electromechanical switch/sensor is fabricated based on the presented seedless synthesis method to demonstrate the application potential of this method.

Fig. 5(a) shows a schematic diagram of the electromechanical switch/sensor. Chromium was used as an adhesion layer and
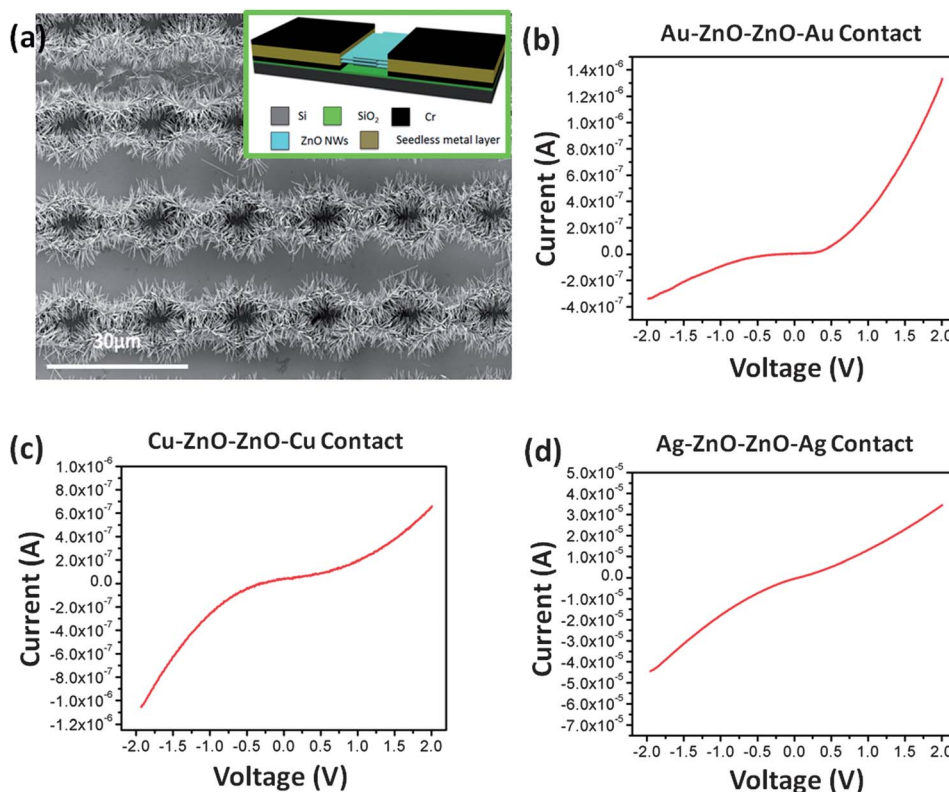

Fig. 4 I–V curves revealing the characteristics of the contacts formed between the ZnO NWs and the underlying metal layer. (a) An SEM image showing the contact of the NWs from the two sides of the electrodes after the growth step. The scale bar is 30 μm. The inset is a schematic diagram of the as-fabricated device used for the electrical measurements. (b) The I–V curve for the Au-ZnO-ZnO-Au contact, showing the rectifying character of Schottky contact. (c) The I–V curve for the Cu-ZnO-ZnO-Cu contact, showing weaker rectifying character of Schottky contact. (d) The I–V curve for the Ag-ZnO-ZnO-Ag contact, showing the weakest rectification characters among the three.

a capping layer. 10 nm chromium, 200 nm silver and 20 nm chromium were deposited in sequence. After the metals were patterned onto the PET substrate, the substrate was placed face down on top of the solution of 100 ml 20mM $Zn(NO_3)_2 \cdot 6H_2O$ and 5 ml ammonia hydroxide (28 wt%), all of which were contained in a 500 ml container. Synthesis was carried out at 95 °C for 5 h. The inset of Fig. 5(a) shows the contacts of the NWs from both sides of the electrodes after the growth step. The device was subsequently connected with conductive wires and sealed/packaged using

polydimethylsiloxane (PDMS) to increase the mechanical robustness of the device. One end of the device was fixed onto a sample holder with the other end free. The free end was then pushed and released by a computer controlled linear motor, which applies strain to the device.

A set of I–V curves under different strains with the voltage sweeping between −5 V and 5 V is shown in Fig. 5(c). Strain is calculated using the method reported elsewhere.[31] Under zero strain, NWs from the two sides are in maximum contact with each other. By
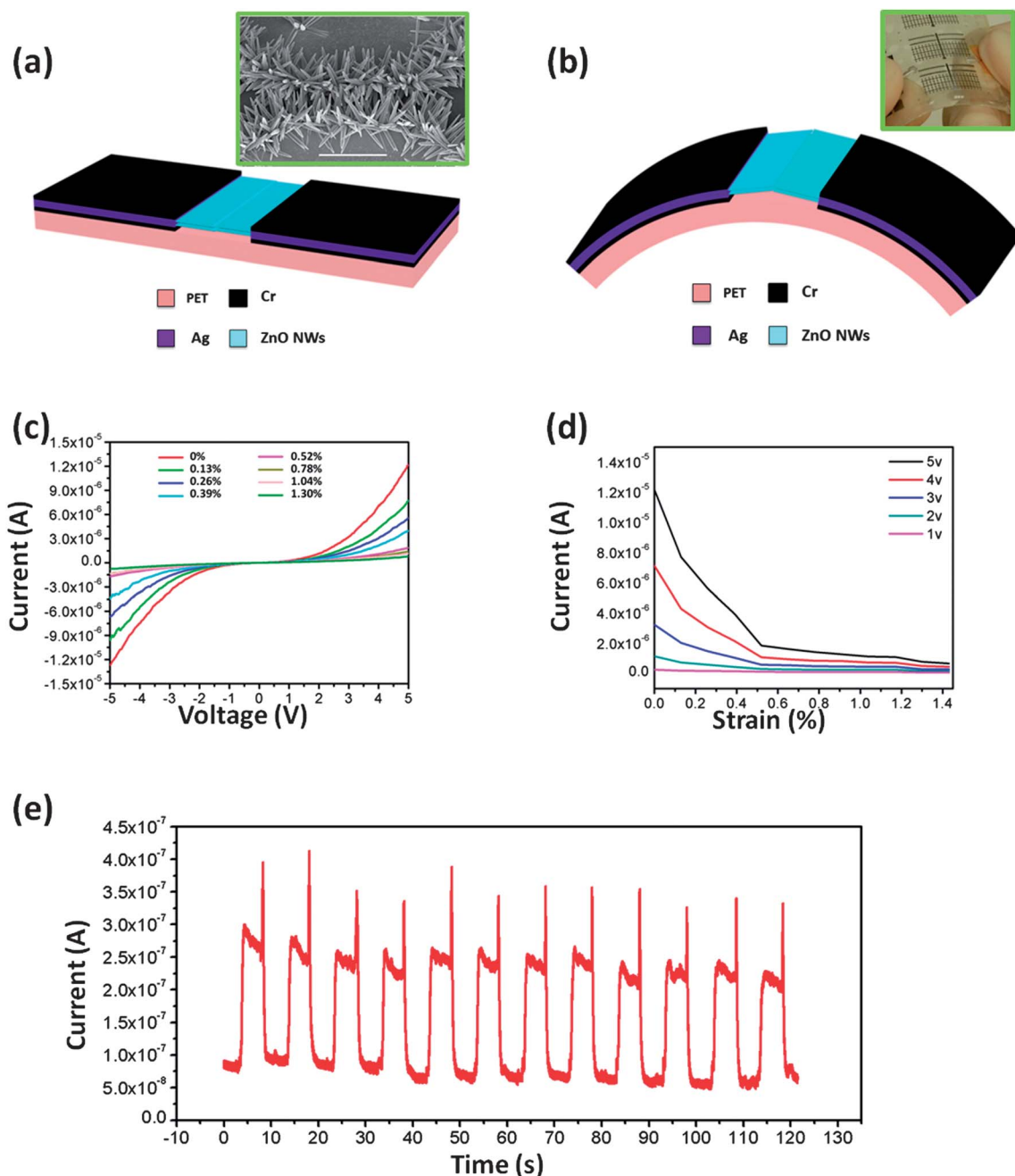

Fig. 5 Electromechanical switch/sensor fabricated with the presented synthesis method on flexible PET substrates. (a) A schematic diagram of the electromechanical switch/sensor. The inset shows the contact of the NWs from two sides of the electrodes after the growth step. The scale bar is 15 μm. (b) A schematic diagram showing the working principle of the device. The inset is an optical image of the as-fabricated device. (c) A set of I–V curves obtained under different applied strains. (d) A set of strain response curves (current–strain curves) obtained under different fixed bias voltages. (e) On/off performance of the device at a fixed bias voltage of 2 V over a period of 120 s.

applying a tensile strain, NWs from one side will start to detach from the NWs on the other side and the current flowing through the device will start to drop, due to fewer contacts between the NWs of the two sides and hence a larger resistance. This working principle is schematically shown in Fig. 5(b). Considering the device under 0% strain as being in the "on" state and the device under 1.3% strain as being in the "off" state, the on/off ratio is approximately 20. Fig. 5(d) shows a set of strain response curves (current–strain curves) under different fixed bias voltages. The response is more sensitive at low strain values, meaning that the current drops very fast initially and will decrease more and more slowly with increasing strain. This response characteristic is consistent with the device structure in that the contact of NWs, which are located well above the PET substrate surface, could be easily broken at a relatively low strain but for NWs located very close to the PET substrate surface, the contact will remain until a very high strain is applied. This measurement result is analogous to the I_{ds}–V_g transfer curve used to characterize a field effect transistor (FET). The difference is that the electrical gate voltage used in the FET is replaced by the applied mechanical strain in this device, which controls the conductivity of the conducting channel. Fig. 5(e) shows the on–off performance of the device at a fixed bias voltage of 2 V. The device is pushed and released by a linear motor every five seconds and the current data is recorded over a period of 120 s.

Most NW based electromechanical switches and strain sensors reported thus far are single wire devices. The fabrication strategy is to first grow NWs and then transfer them from growth substrates to device substrates for further fabrication, like the patterning/deposition of electrodes, which takes effort to determine the position of the distributed NWs. Highly ordered NW assembly is needed for scaled-up applications such as sensor arrays. The electromechanical switch/sensor reported in this work adopts a reverse strategy. Electrodes are first made with simple techniques and NWs are subsequently grown from the pre-defined areas directly. No further complex fabrication steps are needed after the NW growth and this advantage makes it possible to realize semiconductor NW array based applications at a large scale.

3. Conclusions

In summary, we have demonstrated a method to grow dense and aligned ZnO NW arrays on various patterned metal layers without pre-depositing a seed layer. The effects of ammonia concentration (a/n volume ratio) and solution/container volume ratio (s/c volume ratio) on the NW growth have been investigated in detail and the proposed growth mechanism has been discussed. The strong nucleation for preferential NW growth has been demonstrated by using substrates with patterned layers of various metals. The contact between the as-grown NWs and metal layers has been electrically characterized. Finally, an electromechanical switch/sensor based on PET substrates utilizing the presented synthesis method was fabricated. This novel hydrothermal synthesis approach demonstrates the capability of seedless growth of ZnO NWs on various substrates, enabling the potential applications of ZnO NW arrays for sensing, electromechanical actuation and energy harvesting, *etc.*

Experimental

(100) silicon wafers and PET substrates (with a thickness of 500 μm) were used in this work. 200 nm of SiO_2 layer was thermally grown (Tystar Polysilicon tube furnace) on the silicon wafer, serving as the insulating layer. A thin layer of 10 nm Cr was subsequently deposited as the adhesion layer before the deposition of a 200 nm thick metal layer. In the case of the gold layer, an extra annealing process at 500 °C for 5 min in a rapid thermal processor (RTP) was carried out to improve the crystallinity of the gold film.

The two precursor chemicals involved in the synthesis are zinc nitrate hexahydrate ($Zn(NO_3)_2 \cdot 6H_2O$, 98%, reagent grade, Sigma Aldrich) and ammonium hydroxide ($NH_3 \cdot H_2O$, 28%–30% wt%, reagent grade, Sigma Aldrich). In the work presented here, the nutrient solution was prepared to keep the concentration of $Zn(NO_3)_2 \cdot 6H_2O$ at 20 mM while the concentration of ammonia was varied. The substrate for NW growth was put face-down floating on top of the solution, taking advantage of the surface tension, and NW growth was achieved in a Yamato convection oven at 95 °C for 5 h.

Patterned metal layers on both silicon and PET substrates were fabricated by standard photo-lithography, electron beam evaporation and subsequent lift-off processes. Except for gold, all of the other metals used do not require RTP treatment to achieve NW growth. The as-grown samples were subsequently examined at 10 kV with a LEO scanning electron microscope (SEM) and at 380 kV with a JEOL-4000 high-resolution transmission electron microscope (HRTEM). Electrical measurements were performed with a function generator (Model No.: DS345, Stanford Research Systems, Inc.) and a current preamplifier (Model No.: SR560, Stanford Research Systems, Inc.).

References

1 Z. L. Wang, *Mater. Sci. Eng., R*, 2009, **64**, 33–71.
2 Z. L. Wang, *Chin. Sci. Bull.*, 2009, **54**, 4021–4034.
3 L. N. Dem'yanets, D. V. Kostomarov and I. P. Kuz-mina, *Inorg. Mater.*, 2002, **38**, 124–131.
4 K. Govender, D. S. Boyle, P. B. Kenway and P. O'Brien, *J. Mater. Chem.*, 2004, **14**, 2575–2591.
5 S. Xu, C. Xu, Y. Liu, Y. F. Hu, R. S. Yang, Q. Yang, J. H. Ryou, H. J. Kim, Z. Lochner, S. Choi, R. Dupuis and Z. L. Wang, *Adv. Mater.*, 2010, **22**, 4749.
6 X. M. Zhang, M. Y. Lu, Y. Zhang, L. J. Chen and Z. L. Wang, *Adv. Mater.*, 2009, **21**, 2767.
7 A. B. Djurisic, A. M. C. Ng and X. Y. Chen, *Prog. Quantum Electron.*, 2010, **34**, 191–259.
8 M. H. Huang, S. Mao, H. Feick, H. Q. Yan, Y. Y. Wu, H. Kind, E. Weber, R. Russo and P. D. Yang, *Science*, 2001, **292**, 1897–1899.
9 J. K. Song, U. Willer, J. M. Szarko, S. R. Leone, S. Li and Y. Zhao, *J. Phys. Chem. C*, 2008, **112**, 1679–1684.
10 M. Law, L. E. Greene, J. C. Johnson, R. Saykally and P. D. Yang, *Nat. Mater.*, 2005, **4**, 455–459.
11 Y. G. Wei, C. Xu, S. Xu, C. Li, W. Z. Wu and Z. L. Wang, *Nano Lett.*, 2010, **10**, 2092–2096.
12 J. B. Baxter and E. S. Aydil, *Appl. Phys. Lett.*, 2005, **86**, 053114.
13 S. Xu, Y. Qin, C. Xu, Y. G. Wei, R. S. Yang and Z. L. Wang, *Nat. Nanotechnol.*, 2010, **5**, 366–373.
14 X. Zuo, W. Gao, G. Zhang, J. Zhao, Y. Zhu and D. Xia, *Appl. Math. Inform. Sci.*, 2011, **5**, 243–250.
15 X. D. Wang, J. H. Song, J. Liu and Z. L. Wang, *Science*, 2007, **316**, 102–105.

16 Z. L. Wang, *J. Phys. Chem. Lett.*, 2010, **1**, 1388–1393.
17 Z. L. Wang, *Nano Today*, 2010, **5**, 540–552.
18 D. Byrne, R. F. Allah, T. Ben, D. G. Robledo, B. Twamley, M. O. Henry and E. McGlynn, *Cryst. Growth Des.*, 2011, **11**, 5378–5386.
19 H. J. Fan, F. Fleischer, W. Lee, K. Nielsch, R. Scholz, M. Zacharias, U. Gosele, A. Dadgar and A. Krost, *Superlattices Microstruct.*, 2004, **36**, 95–105.
20 X. D. Wang, J. H. Song, P. Li, J. H. Ryou, R. D. Dupuis, C. J. Summers and Z. L. Wang, *J. Am. Chem. Soc.*, 2005, **127**, 7920–7923.
21 M. Willander, O. Nur, Q. X. Zhao, L. L. Yang, M. Lorenz, B. Q. Cao, J. Z. Perez, C. Czekalla, G. Zimmermann, M. Grundmann, A. Bakin, A. Behrends, M. Al-Suleiman, A. El-Shaer, A. C. Mofor, B. Postels, A. Waag, N. Boukos, A. Travlos, H. S. Kwack, J. Guinard and D. L. Dang, *Nanotechnology*, 2009, **20**, 332001.
22 M. C. Jeong, B. Y. Oh, M. H. Ham, S. W. Lee and J. M. Myoung, *Small*, 2007, **3**, 568–572.
23 M. Guo, P. Diao and S. M. Cai, *J. Solid State Chem.*, 2005, **178**, 1864–1873.
24 L. E. Greene, M. Law, J. Goldberger, F. Kim, J. C. Johnson, Y. F. Zhang, R. J. Saykally and P. D. Yang, *Angew. Chem., Int. Ed.*, 2003, **42**, 3031–3034.
25 Y. G. Wei, W. Z. Wu, R. Guo, D. J. Yuan, S. M. Das and Z. L. Wang, *Nano Lett.*, 2010, **10**, 3414–3419.
26 Q. C. Li, V. Kumar, Y. Li, H. T. Zhang, T. J. Marks and R. P. H. Chang, *Chem. Mater.*, 2005, **17**, 1001–1006.
27 X. D. Wang, J. Zhou, J. H. Song, J. Liu, N. S. Xu and Z. L. Wang, *Nano Lett.*, 2006, **6**, 2768–2772.
28 P. H. Yeh, Z. Li and Z. L. Wang, *Adv. Mater.*, 2009, **21**, 4975.
29 J. Zhou, P. Fei, Y. D. Gu, W. J. Mai, Y. F. Gao, R. Yang, G. Bao and Z. L. Wang, *Nano Lett.*, 2008, **8**, 3973–3977.
30 W. Z. Wu and Z. L. Wang, *Nano Lett.*, 2011, **11**, 2779–2785.
31 W. Z. Wu, Y. G. Wei and Z. L. Wang, *Adv. Mater.*, 2010, **22**, 4711.
32 Z. L. Wang and J. H. Song, *Science*, 2006, **312**, 242–246.
33 Y. Qin, X. D. Wang and Z. L. Wang, *Nature*, 2008, **451**, 809–U805.
34 R. S. Yang, Y. Qin, L. M. Dai and Z. L. Wang, *Nat. Nanotechnol.*, 2009, **4**, 34–39.
35 A. Sugunan, H. C. Warad, M. Boman and J. Dutta, *J. Sol-Gel Sci. Technol.*, 2006, **39**, 49–56.
36 S. Xu, C. Lao, B. Weintraub and Z. L. Wang, *J. Mater. Res.*, 2008, **23**, 2072–2077.
37 G. W. Smith and H. W. Jacobson, *J. Phys. Chem.*, 1956, **60**, 1008–1012.
38 Z. Wang, X. F. Qian, J. Yin and Z. K. Zhu, *Langmuir*, 2004, **20**, 3441–3448.
39 M. M. Santore and N. Kozlova, *Langmuir*, 2007, **23**, 4782–4791.
40 C. K. Xu, P. Shin, L. L. Cao and D. Gao, *J. Phys. Chem. C*, 2010, **114**, 125–129.
41 S. Xu, Y. Wei, M. Kirkham, J. Liu, W. Mai, D. Davidovic, R. L. Snyder and Z. L. Wang, *J. Am. Chem. Soc.*, 2008, **130**, 14958.
42 Y. Qin, R. S. Yang and Z. L. Wang, *J. Phys. Chem. C*, 2008, **112**, 18734–18736.
43 T. Shibata, M. Yagi, H. Nishida, H. Kobayashi and M. Tanaka, *Journal of Turbomachinery*, 2012, **134**, 041012.
44 E. Dimitriadou and K. E. Zoiros, *Opt. Laser Technol.*, 2012, **44**, 600–607.
45 Y. G. Sun and J. A. Rogers, *Adv. Mater.*, 2007, **19**, 1897–1916.